

# MICRO/NANOSCALE TRIBOLOGY OF MEMS MATERIALS, LUBRICANTS AND DEVICES

S. SUNDARARAJAN and B. BHUSHAN

Department of Mechanical Engineering, The Ohio State University, Columbus, Ohio 43210-1107, USA,  
e-mail: bhushan.2@osu.edu

## SUMMARY

Although the field of MEMS has expanded considerably over the last decade, the scale of operation and large surface-to-volume ratio of the devices result in very high retarding forces such as friction and adhesion that seriously undermine the performance and reliability of the devices. These are tribological phenomena that need to be studied and understood at the micro to nanoscales. In addition, materials for MEMS must exhibit good microscale tribological properties. Alternate materials to silicon that exhibit superior tribological properties under harsh operating conditions need to be identified. There is also a need to develop lubricants and identify lubrication methods that are suitable for MEMS. A summary of macro and micro/nanotribological studies of materials and lubricants for use in MEMS devices is presented. In particular, silicon, polysilicon and SiC based materials are studied. Perfluoropolyether films and self-assembled monolayers are investigated for lubrication of MEMS. Finally, component level testing of micromotors has also been carried out to aid in better understanding of the observed tribological phenomena in MEMS.

Keywords: MEMS, nanotribology, lubrication, stiction, AFM

## 1 INTRODUCTION - TRIBOLOGICAL ISSUES IN MEMS

Microelectromechanical systems (MEMS) have undergone significant advances over the last two decades with researchers fabricating a variety of miniaturized devices with dimensions ranging from a couple to a few thousand microns [1-2]. Although mostly fabricated using silicon planar lithography based processes, such as bulk micromachining and surface micromachining, MEMS today are also fabricated using non-lithographic micromachining processes such as LIGA (a German term for lithography, electroforming, and plastic moulding) and other laser machining processes [3].

In MEMS devices, various forces associated with the device scale down with the size. When the length of the machine decreases from 1 mm to 1  $\mu\text{m}$ , the area decreases by a factor of million and the volume decreases by a factor of a billion. As a result, surface forces such as friction, adhesion, meniscus forces, viscous drag and surface tension that are proportional to area, become a thousand times larger than the forces proportional to the volume, such as inertial and electromagnetic forces. Since the start-up forces and torques involved in MEMS operation available to overcome retarding forces are small, the increase in resistive forces such as friction and adhesion become serious tribological concerns that limit the life and reliability of MEMS devices [4]. In addition to the consequence of a large surface-to-volume ratio, since MEMS devices are designed for small tolerances, physical contact becomes more likely, which makes them particularly vulnerable to adhesion between adjacent components. A large lateral force required to initiate relative motion between two smooth surfaces is referred to as "stiction", which has been studied extensively in tribology of magnetic storage systems [5]. Friction/stiction (static friction), wear and surface contamination affect device performance and in some cases, can even prevent devices from working.

Figure 1a shows examples of several MEMS devices that can encounter the above-mentioned tribological problems. The polysilicon electrostatic micromotor has 12 stators and a 4-pole rotor and is produced by surface micromachining and is capable of continuous rotation up to speeds of 100,000 rpm. The rotor diameter is 120  $\mu\text{m}$  and the air gap between the rotor and stator is 2  $\mu\text{m}$  [6]. The intermittent contact at the rotor-stator interface and physical contact at the rotor-hub flange interface result in wear issues, and high stiction between the contacting surfaces limits the repeatability of operation or may even prevent the operation altogether. Next is an SEM micrograph of a surface micromachined polysilicon gear train for an air turbine [7]. Wear at the gear teeth is a concern. Commercially available MEMS devices may exhibit tribological problems as well. Figure 1b shows a digital micromirror device (DMD) pixel for xerographic type printers and digital projection displays [8]. It consists of an array of rotatable aluminum mirrors fabricated on top of a CMOS static random access memory integrated circuit. The surface micromachined array consist of a half of a million to a million or more of these independently controlled reflective, digital light switches. The electrostatically activated pixel strikes the electrode surface with a certain amount of energy. Contact between the yoke and the electrode surface is required for true digital (binary) operation. Stiction and wear during these contacts are the issues affecting the reliable operation of the micromirror device [9]. An electrostatically driven, surface-micromachined rotary microactuator for a magnetic disk drive is shown in Fig. 1b [10]. This high-bandwidth servo-controlled microactuator is being developed for ultrahigh-track-density applications [10 - 12]. Actuation is accomplished via capacitive parallel plates, which are alternately attached to the rotor and stator in to form pairs as shown in Fig. 1b. A voltage applied across these plates results in an electrostatic force, which rotates the central rotor. Any unintended contacts

between the rotor and stator plates may result in wear and stiction. Also shown in Fig. 1b is a surface micromachined integrated capacitive silicon accelerometer fabricated by Analog Devices, which is used for automotive sensory applications [13 - 14] (for more information on Analog Devices, visit [www.analog.com](http://www.analog.com)). The central suspended beam mass is supported on the four corners by spring structures. The central beam has interdigitated plates on the four sides that alternate with those of the stationary plates as shown. Motion of the central beam causes a change in the capacitance between these plates, which is used to measure the acceleration. Here stiction of the beam structure with the underlying substrate as well as stiction between the adjacent plates (fingers) are detrimental to the operation of the sensor [14]. Wear during unintended contacts of these plates is also a problem. Friction/stiction and wear clearly limit the lifetimes and compromise the performance and reliability of microdevices. Figure 2 summarizes some of the various tribological problems encountered in various MEMS devices and components just discussed. In addition, there are tribological issues in the fabrication processes that are also being addressed. For

example, in surface micromachining, the suspended structures can sometimes collapse and permanently adhere to the underlying substrate due to meniscus effects during the final rinse and dry process [15]. The mechanism of such adhesion phenomena needs to be understood [16 - 17].

It is clear that tribology is an important factor affecting the performance and reliability of MEMS devices. There is a need for development of a fundamental understanding of friction/stiction, wear, and the role of surface contamination and environment in microdevices [4]. MEMS materials need to exhibit good tribological and mechanical properties on the micro/nanoscales. There is a need to develop lubricants and identify lubrication methods that are suitable for MEMS. Component-level studies are also required to provide a better understanding of the tribological phenomena occurring in MEMS. The emergence of micro/ nanotribology and atomic force microscopy-based techniques has provided researchers a viable approach to solve these problems [18 - 19]. The following is a review of macro- and micro/nanoscale tribological studies of MEMS materials, lubricants and devices.

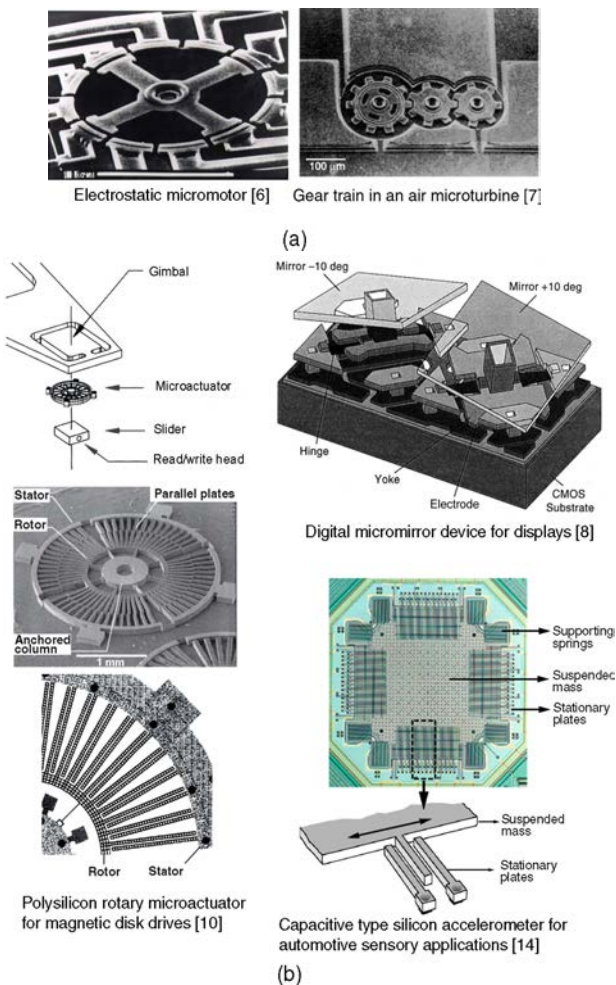


Figure 1: Examples of MEMS devices encountering tribological problems; (a) early research devices and (b) devices with commercial applications.

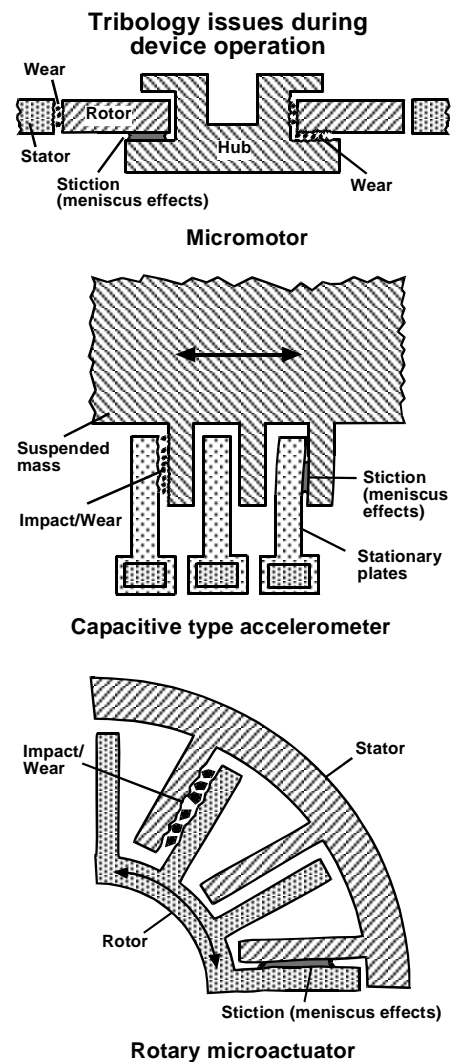


Figure 2: Summary of tribological issues in MEMS device operation

## 2 TRIBOLOGICAL STUDIES OF MEMS MATERIALS

Materials of most interest for planar fabrication processes using silicon as the structural material are undoped and boron-doped ( $p^+$ -type) single-crystal silicon for bulk micromachining and phosphorus ( $n^+$ -type) doped and undoped LPCVD polysilicon films for surface micromachining. Alternate materials to complement silicon in MEMS need to be identified. Silicon-based MEMS devices lack high-temperature capabilities with respect to both mechanical and electrical properties. Researchers have been pursuing SiC as a material for high-temperature microsensor and micro-actuator applications for some time [20 - 21] based on its success in high-temperature electronics and high-power devices. Table 1 compares selected bulk properties of SiC and Si(100). Researchers have found low-cost techniques of producing single-crystal 3C-SiC (cubic or  $\beta$ -SiC) films via epitaxial growth on large area silicon substrates for bulk micromachining [22] and polycrystalline 3C-SiC films on polysilicon and silicon dioxide layers for surface micromachining of SiC [23]. It is believed that these films will be well suited for MEMS devices if it can exhibit good microtribological properties. As will be shown, bare silicon exhibits inadequate tribological performance and needs to be coated with a solid and/or liquid overcoat or be surface treated (e.g. oxidation, commonly used in semiconductor manufacturing), which exhibits lower friction

and wear. Both macroscale and microscale tribological studies are described.

### 2.1 Virgin and Treated/Coated Silicon Samples

#### 2.1.1 Tribological properties of silicon and effect of ion-implantation

Friction and wear of single-crystalline and polycrystalline silicon samples were studied and the effect of ion implantation with various doses of  $C^+$ ,  $B^+$ ,  $N_2^+$  and  $Ar^+$  ion species at 200 keV energy to improve their friction and wear properties was studied [24 - 26]. The coefficient of macroscale friction and wear factor of virgin single-crystal silicon and  $C^+$ -implanted silicon samples as a function of ion dose are presented in Fig. 3 [24]. The macroscale friction and wear tests were conducted using a ball-on-flat tribometer. Each data bar represents the average value of four to six measurements. The coefficient of friction and wear factor for bare silicon are very high and these decrease drastically with ion dose. Silicon samples bombarded above  $10^{17} C^+ cm^{-2}$  exhibit extremely low values of coefficients of friction (typically 0.03 to 0.06 in air) and the wear factor (reduced by as much as four orders of magnitude). A decrease in coefficient of friction and wear factor of silicon as a result of  $C^+$  ion bombardment occurred because of formation of silicon carbide rather than amorphization of silicon [24]. An improvement in friction and wear with  $B^+$  ion implantation was also reported [24].

Sample	Density (kg/m <sup>3</sup> )	Hardness (GPa)	Elastic modulus (GPa)	Fracture toughness (MPa m <sup>1/2</sup> )	Thermal conductivity <sup>b</sup> (W/m K)	Coefficient of thermal expansion <sup>b</sup> ( $\times 10^{-6} / ^\circ C$ )	Melting point ( $^\circ C$ )	Band-gap (eV)
$\beta$ -SiC	3210	23.5-26.5	440	4.6	85-260	4.5 - 6	2830	2.3
Si(100)	2330	9-10	130	0.95	155	2 - 4.5	1410	1.1

Table 1: Selected bulk properties of 3C ( $\beta$ - or cubic) SiC and Si(100).

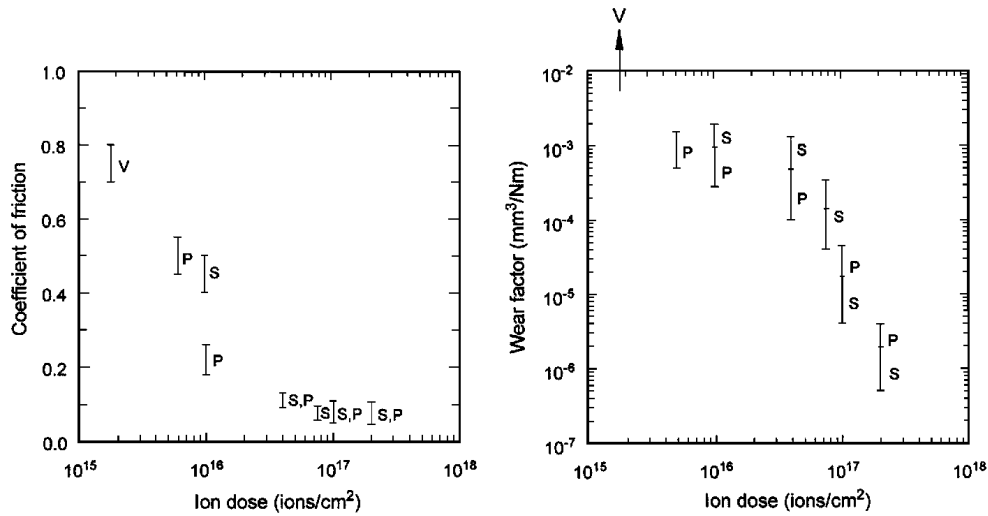


Figure 3: Influence of ion doses on the coefficient of friction and wear factor on  $C^+$  ion bombarded single-crystal and polycrystalline silicon slid against alumina ball. V corresponds to virgin single-crystal silicon, while S and P denote tests that correspond to doped single- and polycrystalline silicon, respectively [24].

Microscale friction measurements were performed using an atomic force/friction force microscope (AFM/FFM) [19]. The studies showed a decrease in microscale and macroscale friction as a result of ion implantation. Results of microscale wear resistance studies of ion-implanted silicon samples studied using a diamond tip in an AFM [27] are shown in Fig. 4a.

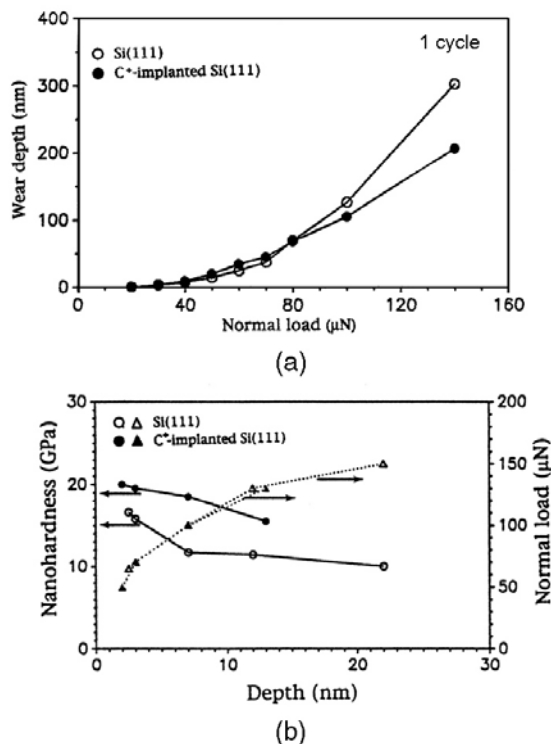


Figure 4: (a) Wear depth as a function of load after one cycle for and (b) Nanohardness and normal load as a function of indentation depth for virgin and C<sup>+</sup> - implanted Si(111) [27].

For tests conducted at various loads on Si(111) and C<sup>+</sup>-implanted Si(111), it is noted that wear resistance of implanted sample is slightly poorer than that of virgin silicon up to about 80  $\mu\text{N}$ . Above 80  $\mu\text{N}$ , the wear resistance of implanted Si improves. As one continues to run tests at 40  $\mu\text{N}$  for a larger number of cycles, the implanted sample exhibits higher wear resistance than the unimplanted sample. Damage from the implantation in the top layer results in poorer wear resistance; however, the implanted zone at the subsurface is more wear resistant than the virgin silicon. Hardness values of virgin and C<sup>+</sup> -implanted Si(111) at various indentation depths (normal loads) are presented in Fig. 4b [27]. The hardness at a small indentation depth of 2.5 nm is 16.6 GPa and it drops to a value of 11.7 GPa at a depth of 7 nm and a normal load of 100  $\mu\text{N}$ . Higher hardness values obtained in low-load indentation may arise from the observed pressure-induced phase transformation during the nanoindentation [28, 29]. Additional increase in the hardness at an even lower indentation depth of 2.5 nm reported here may arise from the contribution by complex chemical films (not from native oxide films) present on the silicon surface. At small volumes there is

a high probability that indentation would be made into a region that was initially dislocation free. Furthermore, at small volumes, it is believed that there is an increase in the stress necessary to operate dislocation sources [30]. If the silicon material were to be used at very light loads such as in microsystems, the high hardness of surface films would protect the surface until it is worn. Figure 4b shows that ion implantation with C<sup>+</sup> results in an increase in hardness in silicon. Note that the surface layer of the implanted zone is much harder compared with the subsurface, and may be brittle leading to higher wear on the surface. The subsurface of the implanted zone is harder than the virgin silicon, resulting in higher wear resistance, which is also seen in the results of the macroscale tests conducted at high loads.

### 2.1.2 Effect of oxidation on tribological properties of silicon

Macro-scale friction and wear experiments have been performed using a magnetic disk drive with bare, oxidized, and implanted pins sliding against amorphous carbon coated magnetic disks lubricated with a thin layer of perfluoropolyether lubricant [31 - 34]. Dry-oxidized Si(111) exhibits excellent characteristics and no significant increase in coefficient of friction was observed over 50,000 cycles whereas changes in frictional behaviour of bare silicon was observed within 5000 cycles. This behaviour has been attributed to the chemical passivity of the oxide and lack of transfer of DLC from the disk to the pin. The behaviour of PECVD-oxide was comparable to that of dry oxide but for the wet oxide there was a 50 % variation in the coefficient of friction. The difference between dry and wet oxide was attributed to increased porosity of the wet oxide [31]. Based on macroscale tests using disk drives, it is found that the friction and wear performance of bare silicon is not adequate. With dry-oxidized or PECVD SiO<sub>2</sub>-coated silicon, no significant friction increase or interfacial degradation was observed in ambient air.

Table 2 shows microscale friction and scratch data for the various silicon samples [27]. Scratch experiments were performed using a diamond tip in an AFM. Results on polysilicon samples are also shown for comparison. Coefficients of microscale friction values for all the samples are about the same. Scratch depth increased with normal load. Crystalline orientation of silicon has little influence on scratch resistance because natural oxidation of silicon in ambient masks the expected effect of crystallographic orientation. PECVD-oxide samples showed the best scratch resistance, followed by dry-oxidized, wet-oxidized, and ion-implanted samples. Ion implantation with P<sup>+</sup> does not appear to improve scratch resistance. Wear data on the silicon samples are also presented in Table 2 [27]. PECVD-oxide samples showed superior wear resistance followed by dry-oxidized, wet-oxidized, and ion-implanted samples. This agrees with the trends seen in scratch resistance. In PECVD, ion bombardment during the deposition improves the coating properties such as suppression of columnar growth, freedom from pinhole, decrease in

Material	Rms roughness <sup>a</sup> (nm)	Coefficient of microscale friction <sup>b</sup>	Scratch depth <sup>c</sup> at 40 $\mu$ N (nm)	Wear depth <sup>c</sup> at 40 $\mu$ N (nm)	Nano-hardness <sup>c</sup> at 100 $\mu$ N (GPa)
Si(111)	0.11	0.03	20	27	11.7
Si(110)	0.09	0.04	20		
Si(100)	0.12	0.03	25		
Polysilicon	1.07	0.04	18		
Polysilicon (lapped)	0.16	0.05	18	25	12.5
PECVD-oxide coated Si(111)	1.50	0.01	8	5	18.0
Dry-oxidized Si(111)	0.11	0.04	16	14	17.0
Wet-oxidized Si(111)	0.25	0.04	17	18	14.4
C <sup>+</sup> -implanted Si(111)	0.33	0.02	20	23	18.6

<sup>a</sup> Scan size of 500 nm x 500 nm using AFM

<sup>b</sup> Versus Si<sub>3</sub>N<sub>4</sub> tip in AFM/FFM, radius 50 nm; at 1  $\mu$ m x 1  $\mu$ m scan size

<sup>c</sup> Measured using an AFM with a diamond tip of radius of 100 nm

Table 2: RMS, microfriction, microscratching/microwear and nanoindentation hardness data for various virgin, coated and treated silicon samples.

crystalline size, and increase in density, hardness and substrate-coating adhesion. These effects may help in improving mechanical integrity of the sample surface. Coatings and treatments improved nanohardness of silicon. Note that dry-oxidized and PECVD films are harder than wet-oxidized films as these films may be porous. High hardness of oxidized films may be responsible for measured high scratch/wear resistance.

## 2.2 Tribological Studies of Polysilicon Films and SiC Films

Studies have also been conducted on undoped polysilicon film, heavily doped (n<sup>+</sup>-type) polysilicon film, heavily doped (p<sup>+</sup>-type) single-crystal Si(100) and 3C-SiC (cubic or  $\beta$ -SiC) film [35 - 37]. The polysilicon films studied here are different from the ones discussed previously in Section 2.1.

Table 3 presents a summary of the tribological studies conducted on polysilicon and SiC films. Values for single-crystal silicon are also shown for comparison. Polishing of the as-deposited polysilicon and SiC films drastically affect the roughness as the values reduce by two orders of magnitude. Si(100) appears to be the smoothest followed by polished undoped polysilicon and SiC films, which have comparable roughness. The doped polysilicon film shows higher roughness than the undoped sample, which is attributed to the doping process. Polished SiC film shows the lowest friction followed by polished, undoped polysilicon film, which strongly supports the candidacy of SiC films for use in MEMS devices. Macroscale friction measurements indicate that SiC film exhibits one of the lowest friction values as compared to the other samples. Doped polysilicon sample shows low friction on the macroscale as compared to the undoped polysilicon sample.

Sample	Rms roughness <sup>a</sup> (nm)	P-V distance <sup>a</sup> (nm)	Coefficient of friction		Scratch depth <sup>d</sup> (nm)	Wear depth <sup>e</sup> (nm)	Nano-hardness <sup>f</sup> (GPa)	Young's modulus <sup>f</sup> (GPa)	Fracture toughness <sup>g</sup> K <sub>IC</sub> MPa m <sup>1/2</sup>
			Micro <sup>b</sup>	Macro <sup>c</sup>					
Undoped Si(100)	0.09	0.9	0.06	0.33	89	84	12	168	0.75
Undoped polysilicon film (as deposited)	46	340	0.05						
Undoped polysilicon film (polished)	0.86	6	0.04	0.46	99	140	12	175	1.11
n <sup>+</sup> -Type polysilicon film (as deposited)	12	91	0.07						
n <sup>+</sup> -Type polysilicon film (polished)	1.0	7	0.02	0.23	61	51	9	95	0.89
SiC film (as deposited)	25	150	0.03						
SiC film (polished)	0.89	6	0.02	0.20	6	16	25	395	0.78

<sup>a</sup> Measured using AFM over a scan size of 10  $\mu$ m x 10  $\mu$ m

<sup>b</sup> Measured using AFM/FFM over a scan size of 10  $\mu$ m x 10  $\mu$ m

<sup>c</sup> With a 3-mm diam. sapphire ball in reciprocating mode, normal load of 10 mN, average sliding speed of 1 mm/s after 4 m sliding distance

<sup>d</sup> Measured using AFM at a normal load of 40  $\mu$ N for 10 cycles, scan length of 5  $\mu$ m

<sup>e</sup> Measured using AFM at normal load of 40  $\mu$ N for 1 cycle

<sup>f</sup> Measured using Nanoindenter at a peak indentation depth of 20 nm

<sup>g</sup> Measured using microindenter (Vickers) at a normal load of 0.5 N

Table 3: Summary of micro/nanotribological properties of the sample materials.

This may possibly be due to the doping effect. Figure 5a shows a plot of scratch depth vs. normal load for various samples [35 - 36]. Scratch depth increases with increasing normal load. It can be seen that scratch depth increases almost linearly with the normal load. Si(100) and the doped and undoped polysilicon film show similar scratch resistance. From the data, it is clear that the SiC film is much more scratch resistant than the other samples. Figure 5b shows results from microscale wear tests on the various films. For all the materials, the wear depth increases almost linearly with increasing number of cycles. This suggests that the material is removed layer by layer in all the materials. Here also, SiC film exhibits lower wear depths than the other samples. Doped polysilicon film wears less than the undoped film. Higher fracture toughness and higher hardness of SiC as compared to Si(100) is responsible for its lower wear. Also the higher thermal conductivity of SiC (see Table 1) as compared to the other materials leads to lower interface temperatures, which generally results in less degradation of the surface [5,38]. Doping of the polysilicon does not affect the scratch/wear resistance and hardness much. These studies indicate that SiC film exhibits desirable tribological properties for use in MEMS devices. Recently, researchers have fabricated SiC micromotors and have reported satisfactory operation at high temperatures [39].

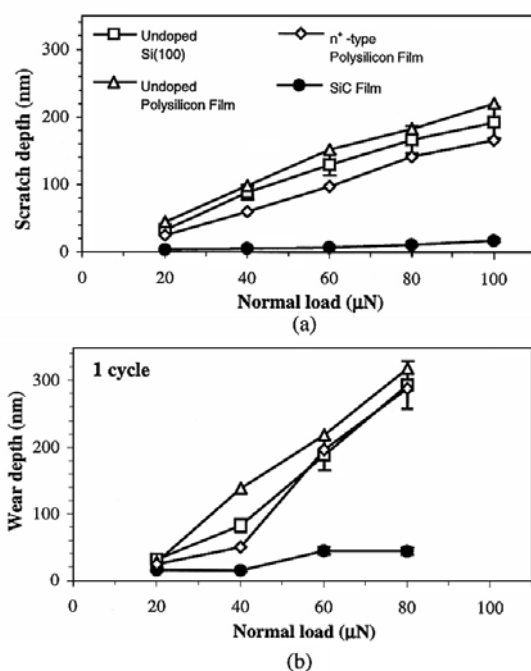


Figure 5: (a) Scratch depths for 10 cycles as a function of normal load and (b) wear depths as a function of normal load for various samples [35].

### 3 TRIBOLOGICAL STUDIES OF LUBRICANTS FOR MEMS

Several studies of liquid perfluoropolyether (PFPE) lubricants, Langmuir-Blodgett (L-B) films and self-assembled monolayers (SAMs) have been carried out to minimize friction and wear [9, 19, 40 - 43]. These are described here.

#### 3.1 Perfluoropolyether Lubricants

The classical approach to lubrication uses freely supported multimolecular layers of liquid lubricants. The liquid lubricants are chemically bonded to improve their wear resistance. Liquid perfluoropolyether lubricants are widely used in magnetic hard disks and may be suitable for MEMS devices. Results from microscale friction measurements performed using an AFM/FFM as a function of number of cycles on virgin Si(100) and silicon lubricated with about 2-nm-thick Z-15 and Z-DOL PFPE lubricants are shown in Fig. 6 [41]. Z-DOL is a PFPE lubricant with hydroxyl end groups. Its lubricant film was thermally bonded at 150° C for 30 minutes and washed off with a solvent to provide a chemically bonded layer for the lubricant film. In Fig. 6, the unlubricated silicon sample showed a slight increase in friction force followed by a drop to a lower steady-state value after 20 cycles. Depletion of native oxide and possible roughening of the silicon sample are believed to be responsible for the decrease in friction force after 20 cycles. The initial friction force for Z-15 lubricated sample is lower than that of unlubricated silicon and increases gradually to a friction force value comparable to that of unlubricated silicon after 20 cycles. This suggests depletion of the Z-15 lubricant in the wear track. In the case of the Z-DOL-coated sample, the friction force starts out to be low and remains low during the cycle of 100 tests. It suggests that Z-DOL does not get displaced or depleted as readily as Z-15. Additional studies of freely supported liquid lubricants showed that either increasing the film thickness or chemically bonding the molecules to the substrate with a mobile fraction improves the lubrication performance [41-42].

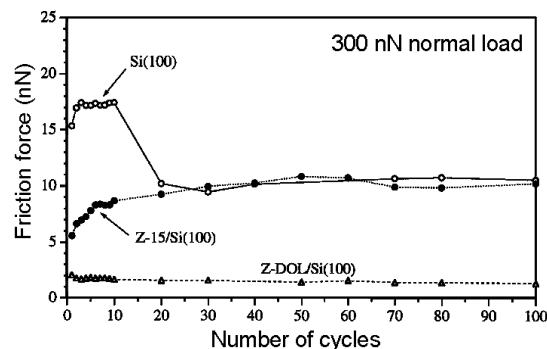


Figure 6: Friction force as a function of number of cycles using an  $\text{Si}_3\text{N}_4$  tip at 300 nN normal load for unlubricated and lubricated silicon samples [41].

#### 3.2 Langmuir-Blodgett Films and Self-Assembled Monolayers

A preferred method of lubrication of microdevices is by the deposition of organized and dense molecular-scale layers of long-chain molecules, as they have been shown to be superior lubricants on the macroscale [40, 44]. Two common methods to produce monolayers are the Langmuir-Blodgett (L-B) deposition and self-assembled monolayers (SAMs) by chemical grafting of molecules. Microscale tribological studies of L-B films and SAMs

have been carried out using an AFM/FFM [40]. Table 4 lists the coefficients of microscale and macroscale friction values for the various lubricants studied. Figure 7 shows the results of microscale wear tests on grafted octadecyl ( $C_{18}$ ) films and the corresponding  $SiO_2$  substrate and zinc arachidate (ZnA) and octadecyl Thiol (ODT) films and corresponding Au/Si substrate. The grafted film shows lower friction and exhibit better wear resistance than the other films. This is due to their stronger covalent bonding to the substrate as compared to the weak van der Waals bonds between the L-B films and the substrate. The higher durability exhibited by SAMs compared to L-B films suggest that SAMs are the better choice for lubrication of MEMS devices.

Sample	RMS roughness <sup>a</sup> (nm)	Coefficient of friction	
		Micro <sup>b</sup>	Macro <sup>c</sup>
Si(100)	0.12	0.03	0.33
$SiO_2/Si$	0.21	0.03	0.19
$C_{18}$	0.16	0.018	0.07
grafted/ $SiO_2/Si$			
Au/Si	1.16	0.04	0.13
ODT/Au/Si	0.92	0.03	0.14
ZnA/ODT/Au/Si	0.55	0.03	0.16

<sup>a</sup> Using AFM on a  $1 \mu m \times 1 \mu m$  scan area.

<sup>b</sup> With an  $Si_3N_4$  tip of radius of 30-50 nm; normal load of 10-200 nN and scanning speed of  $4 \mu m/s$ .

<sup>c</sup> With an alumina ball of radius 3 mm; normal load of 0.1 N and sliding speed of 0.8 mm/s.

Table 4: Typical RMS roughness and coefficients of microscale and macroscale friction values for various L-B films, chemically grafted films and their substrates.

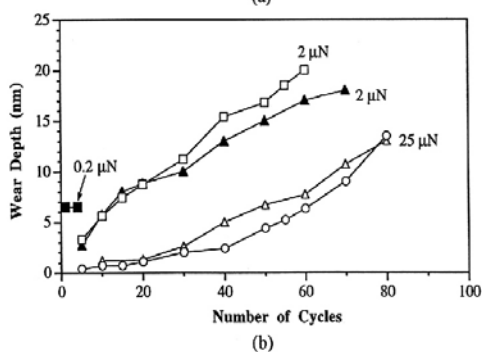
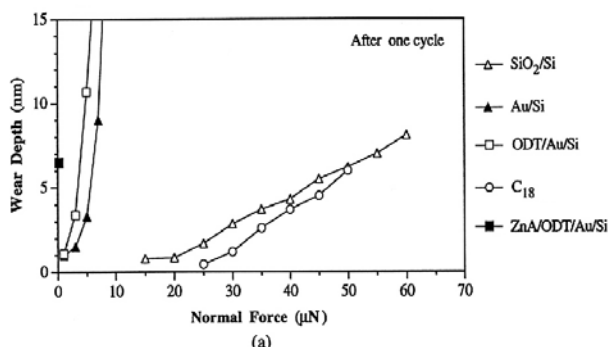


Figure 7: Wear depth as a function of (a) normal load and (b) number of wear cycles of various L-B and grafted films using an AFM [40].

SAMs can be spontaneously formed by immersion of an appropriate substrate into a solution of an active surfactant in an organic solvent. SAMs therefore offer the flexibility and advantage of molecular tailoring to obtain a variety of different tribological and mechanical properties. Various studies indicate that the basis for molecular design and tailoring of SAMs must include a complete understanding of interrelationships between the molecular structure and tribological properties of SAMs, as well as a deep understanding of the friction and wear mechanisms of SAMs at the molecular level. Bhushan and Liu studied nanotribological properties of four different kinds of alkythiol and biphenyl thiol monolayers with different surface terminals, spacer chains and head groups using AFM/FFM techniques [43]. These monolayers along with a schematic of their structures and substrates are listed in Fig. 8.

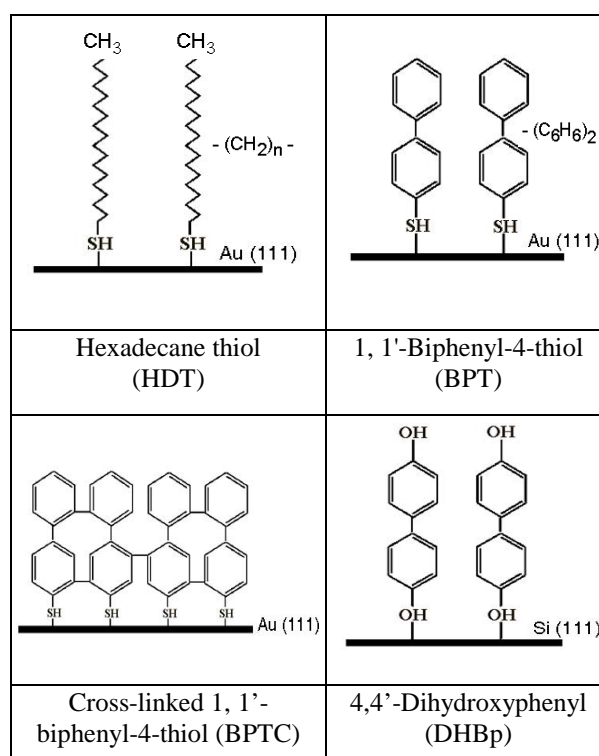


Figure 8: Structure of SAMs studied using AFM [43].

Surface roughness, nanoscale friction and adhesion studies were carried out using an AFM/FFM. Figure 9 shows AFM surface height and corresponding friction force maps of the SAMs studied over a  $1 \mu m^2$  scan area. The films deposited on gold appear to be granular and reproduce the underlying gold substrate well. Cross-linking of BPT via low energy electron radiation results in higher roughness (BPTC). The films deposited on silicon are featureless, indicating that they too reproduce the substrate well. For Au(111), HDT and BPTC, correlations between the surface height and the corresponding friction force maps were attributed to effect of slope [45]. For BPT, it was observed that the high surface height area corresponds to low friction, suggesting a material-based friction effect. For Si(111) and DHBp, the friction force images appear uniform.

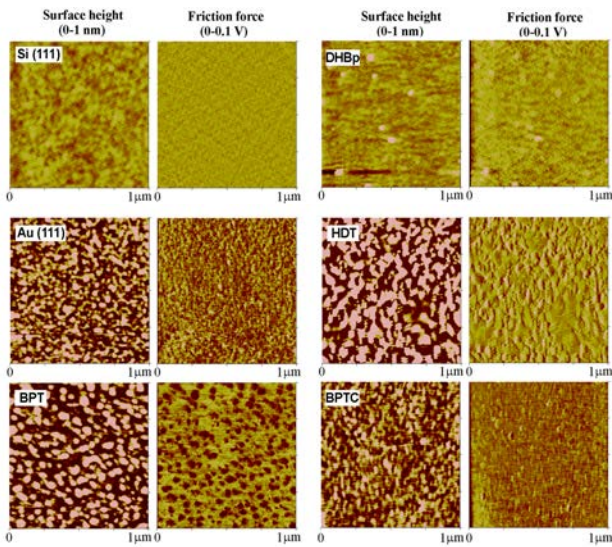
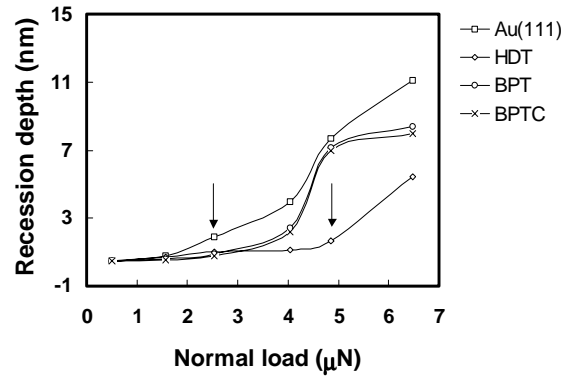
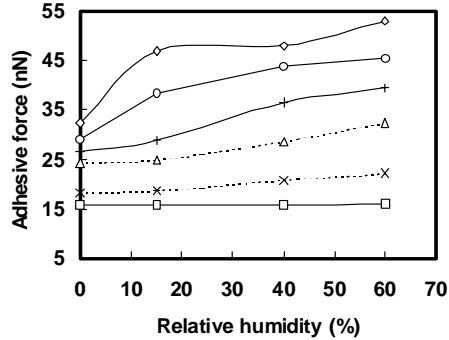
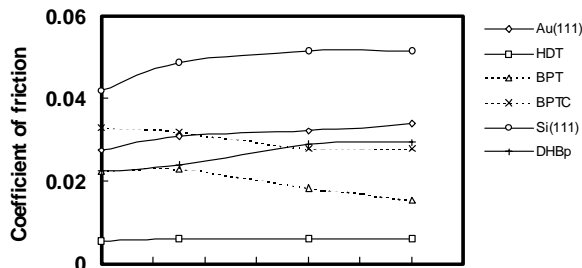


Figure 9: Surface height and corresponding friction force maps of various SAMs along with substrates [43].



(a)



(b)

Figure 10: (a) Coefficient of friction values and (b) effect of relative humidity on adhesive force and coefficient of friction of the SAMs [43].

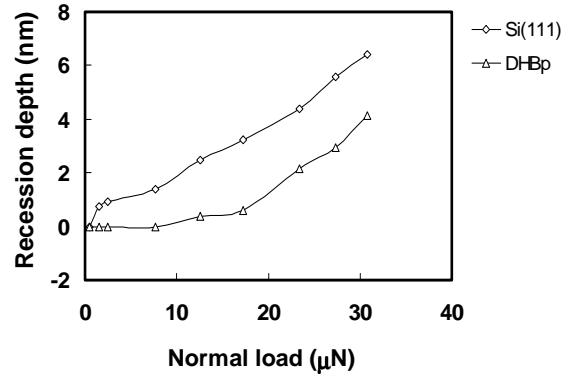


Figure 11: Wear depth as a function of normal load for various SAMs [43].

The coefficient of microscale friction values for the various SAMs and their standard deviation are summarized in Fig. 10a. It shows that alkylthiol and biphenyl thiol SAMs can be used as effective molecular lubricants for silicon in MEMS. The influence of relative humidity on adhesion and friction were studied in an environment control chamber. The results are given in Fig. 10b, which shows that for Si(111), Au(111) and DHBp, the adhesive and frictional forces increase with relative humidity. For BPT and BPTC, the adhesive forces slightly increase with relative humidity when the relative humidity is higher than 40%, but it is very interesting that their coefficients of friction decrease slightly in the same range. For HDT, over the testing range, the adhesive and friction force do not seem to be sensitive to the change in relative humidity. The influence of relative humidity on adhesive and frictional forces can be mainly understood through comparing their surface terminal polarization properties and work of adhesion. Meniscus forces are linearly related to the works of adhesion of a surface, which in the case of SAMs is dependent on the surface terminals. Polar surface terminals, such as DHBp on Si(111), result in higher work of adhesion and hence higher adhesive forces. Larger adhesive forces result in higher friction forces. Non-polar surface terminals (HDT) have very small work of adhesion and hence low adhesive and friction forces. In higher humidity, water capillary condensation can either increase friction through increased adhesion in the contact zone or reduce friction through an enhanced water-lubricating effect. Figure 11 shows results of microscale wear tests on SAMs using a diamond tip in an AFM. DHBp shows the best wear resistance. For all the SAMs tested, there exists a critical

normal load (marked by arrows in Fig. 11). At normal loads higher than the critical load, the wear of the SAMs increase drastically. The wear resistance of SAMs can be influenced by the interface bond strength, the molecular structure of the spacers and the substrate hardness. Bhushan and Liu used a molecular spring model to explain that SAMs exhibit properties that allow them to undergo orientation under normal load [43]. The orientation of SAMs reduced the shearing stress at the interface, allowing SAMs to serve as good durable lubricants. Cross-linking of chains resulted in higher coefficient of friction. According to these results, it is suggested that SAMs that combine the DHBp and HDT molecular structures and are deposited directly on

hydrogenated Si(111) may have optimised tribological performance.

## 4 COMPONENT LEVEL STUDIES

### 4.1 Surface Roughness Studies of Micromotor Components

Most of the friction forces resisting motion in the micromotor are concentrated near the rotor-hub interface where continuous physical contact occurs. Surface roughness of the surfaces usually has a strong influence on the friction characteristics on the micro/nanoscale. Using an AFM, measurements on the various component surfaces can be made.

	RMS Roughness <sup>a</sup> (nm)	Peak-to-Valley Distance <sup>a</sup> (nm)	Skewness <sup>a</sup> , Sk	Kurtosis <sup>a</sup> , K	Coefficient of microscale friction <sup>b</sup> ( $\mu$ )
Rotor Topside	21 $\pm$ 0.6	225 $\pm$ 23	1.4 $\pm$ 0.30	6.1 $\pm$ 1.7	0.07 $\pm$ 0.02
Rotor Underside	14 $\pm$ 2.4	80 $\pm$ 11	-1.0 $\pm$ 0.22	3.5 $\pm$ 0.50	0.11 $\pm$ 0.03
Stator Topside	19 $\pm$ 1	246 $\pm$ 21	1.4 $\pm$ 0.50	6.6 $\pm$ 1.5	0.08 $\pm$ 0.01

<sup>a</sup> Measured from a tapping mode AFM scan of size 5  $\mu\text{m} \times 5 \mu\text{m}$  using a standard Si tip.

<sup>b</sup> Measured using an AFM in contact mode at 5  $\mu\text{m} \times 5 \mu\text{m}$  scan size using a standard Si<sub>3</sub>N<sub>4</sub> tip.

Table 5: Surface roughness parameters and microscale coefficient of friction for various micromotor component surfaces measured using an AFM. Mean and  $\pm 1\sigma$  values are given.

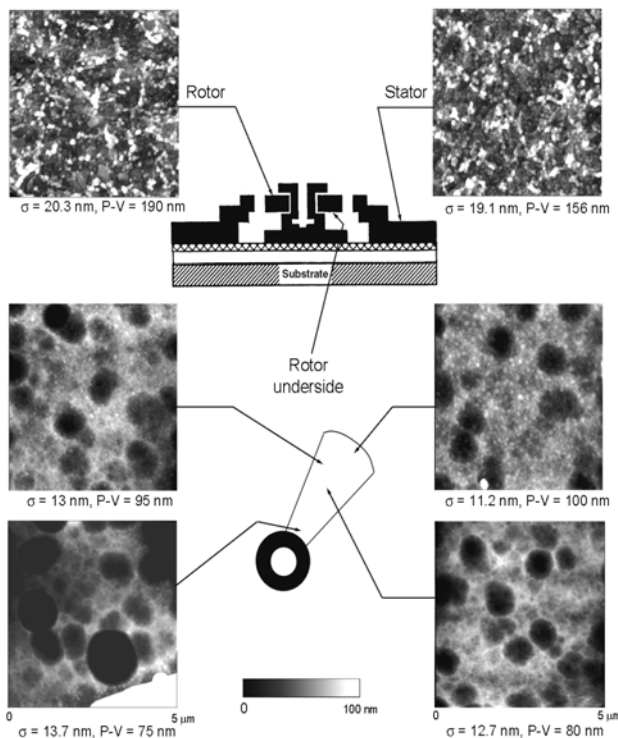


Figure 12: Representative AFM surface height images obtained in tapping mode of various component surfaces of a micromotor. RMS roughness and peak-to-valley values are given. The underside of the rotor exhibits drastically different topography from the topside [51].

Table 5 shows various surface roughness parameters obtained from 5  $\mu\text{m}$  scans of the various component surfaces of several unlubricated micromotors using the AFM in tapping mode. A surface with a Gaussian height distribution should have a skewness of zero and kurtosis of three [38]. Although the rotor and stator top surfaces exhibit comparable roughness parameters, the underside of the rotors exhibits lower RMS roughness and peak-to-valley values. More importantly, the rotor underside shows negative skewness and lower kurtosis than the topsides, both of which are conducive to high real area of contact and hence high friction. The rotor underside also exhibits higher microscale coefficient of friction than the rotor topside and stator. Figure 12 shows representative surface height maps of the various surfaces of a micromotor measured using the AFM in tapping mode. The rotor underside exhibits varying topography from the outer edge to the middle and inner edge. At the outer edges, the topography shows smaller circular asperities, similar to the topside. The middle and inner regions show deep pits with fine edges that may have been created by etching of the sacrificial layer.

Previous studies have also shown that etching can affect the surface roughness of surfaces in surface micromachining [17]. The findings suggest that the surfaces at the rotor-hub interface that come into contact at the end of the fabrication process exhibit large real areas of contact that result in high friction.

## 4.2 Static Friction Force (Stiction) Measurement in MEMS

In MEMS devices involving parts in relative motion to each other, such as micromotors, large friction forces become the limiting factor to the successful operation and reliability of the device. It is generally known that most micromotors cannot be rotated as manufactured and require some form of lubrication. It is therefore critical to determine the friction forces present in such MEMS devices. To measure in-situ the static friction of a rotor-bearing interface in a micromotor, Tai and Muller [46] measured the starting torque (voltage) and pausing position for different starting positions under a constant-bias voltage. A friction-torque model was used to obtain the coefficient of static friction. To measure the in-situ kinetic friction of the turbine and gear structures, Gabriel et al. [47] used a laser-based measurement system to monitor the steady-state spins and decelerations. Lim et al. [48] designed and fabricated a polysilicon microstructure to in-situ measure the static friction of various films.

Beerschwinger's group developed cantilever-deflection rig to measure friction of LIGA-processed micromotors [49 - 50]. Table 6 presents static friction coefficients of various MEMS devices evaluated by various researchers. Most of these techniques employ indirect methods to determine the friction forces or involve fabrication of complex structures. Recently, a novel technique to measure the static friction force (stiction) encountered in surface micromachined polysilicon micromotors using an AFM has been developed [51]. Using this technique, the viability of PFPE lubricants for micromotors has been investigated and the effect of humidity on the friction forces of unlubricated and lubricated devices was studied as well.

Figure 13 shows static friction forces, normalized over the weight of the rotor, of unlubricated and lubricated micromotors as a function of rest time and relative humidity. Rest time here is defined as the time elapsed between the first experiment conducted on a given motor (solid symbol at time zero) and subsequent experiments (open symbols).

Reference	Test method	Device/structure	Material pairs	Environment	Coefficient of static friction
Tai and Muller [45]	Starting voltage	IC-processed micromotor	PolySi/Si <sub>3</sub> N <sub>4</sub>	Air	0.20 - 0.40
Lim et al. [48]	Electrostatic loading	Comb-drive microstructure	PolySi/PolySi PolySi/Si <sub>3</sub> N <sub>4</sub>	Air	4.9 ± 1.0 2.5 ± 0.5
Maboudian [17]	Pull-off force	Silicon microbeams	SiO <sub>2</sub> /SiO <sub>2</sub>	Air	2.1 ± 0.8
Matheison et al. [50]	Cantilever/fiber deflection rig	LIGA micromotors	Ni/Alumina	Air	0.6 - 1.2

Table 6: Published data on coefficient of static friction measurements of MEMS devices and structures.

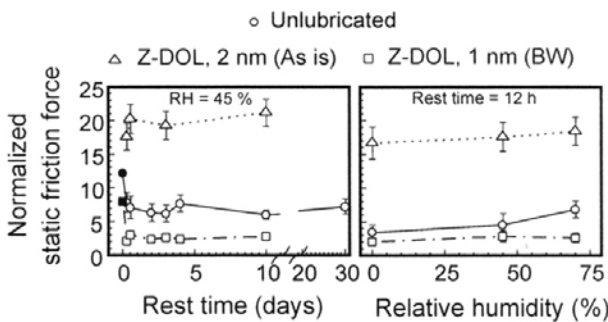


Figure 13: Static friction force values of unlubricated motors and motors lubricated using PFPE lubricants, normalized over the rotor weight, as a function of rest time and relative humidity. Rest time is defined as the time elapsed between a given experiment and the first experiment in which motor movement was recorded (time 0). The motors were allowed to sit at a particular humidity for 12 hours prior to measurements [51].

Each open symbol data point is an average of six measurements. It can be seen that for the unlubricated motor and the motor lubricated with a bonded layer of Z-DOL, the static friction force is highest for the first experiment and then drops to an almost constant level.

In the case of the motor with an as-is mobile layer of Z-DOL, the values remain very high up to 10 days after lubrication. In all cases, there is negligible difference in the static friction force at 0% and 45% RH. At 70% RH, the unlubricated motor exhibits a substantial increase in the static friction force, while the motor with bonded Z-DOL shows no increase in static friction force due to the hydrophobicity of the lubricant layer. The motor with an as-is mobile layer of the lubricant shows consistently high values of static friction force that varies little with humidity.

## 4.3 Mechanisms Associated with Observed Stiction Phenomena in Micromotors

Figure 14 summarizes static friction force data for two motors, M1 and M2 along with schematics of the meniscus effects for the unlubricated and lubricated surfaces. Capillary condensation of water vapour from the environment results in formation of meniscus bridges between contacting and near-contacting asperities of two surfaces in close proximity to each other as shown in Fig. 14. For unlubricated surfaces, more menisci are formed at higher humidity resulting in higher friction force between the surfaces. The form-

ation of meniscus forces is supported by the fact that the static friction force for unlubricated motors increases at high humidity (Fig. 13).

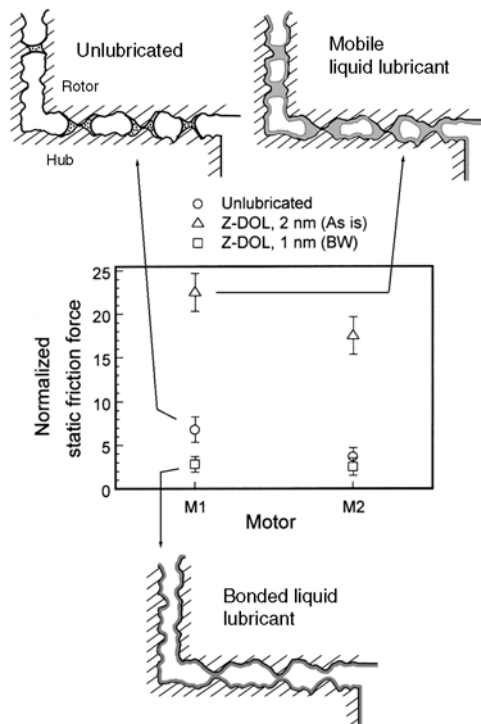


Figure 14: Summary of effect of liquid and solid lubricants on static friction force of micromotors. Despite the hydrophobicity of the lubricant used (Z-DOL), a mobile liquid lubricant (Z-DOL as is) leads to very high static friction force due to increased meniscus forces whereas a solid-like lubricant (bonded Z-DOL) appears to provide some amount of reduction in static friction force.

Solid bridging may occur near the rotor-hub interface due to silica residues after the first etching process [17]. In addition the drying process after the final etch can result in liquid bridging formed by the drying liquid due to capillary force at these areas [16 - 17, 38]. The initial static friction force therefore will be quite high as evidenced by the solid data points in Fig. 13. Once the first movement of the rotor permanently breaks these solid and liquid bridges, the static friction force of the motors will drop (as seen in Fig. 13) to a value dictated predominantly by the adhesive energies of rotor and hub surfaces, the real area of contact between these surfaces and meniscus forces due to water vapour in the air, at which point, effect of lubricant films can be observed. Lubrication with a mobile layer, even a thin one, results in very high static friction forces due to meniscus effects of the lubricant liquid itself at and near the contact regions. It should be noted that a motor submerged in a liquid lubricant would result in a fully flooded lubrication regime. In this case there is no meniscus contribution and only the viscous contribution to the friction forces would be relevant. However, submerging the device in a lubricant may not be a practical method. A solid-like hydrophobic lubricant layer (such as bonded Z-DOL) results in favourable friction

characteristics of the motor. The hydrophobic nature of the lubricant inhibits meniscus formation between the contact surfaces and maintains low friction even at high humidity (Fig. 13). This suggests that solid-like hydrophobic lubricants are ideal for lubrication of MEMS while mobile lubricants result in increased values of static friction force.

## 5 CONCLUSIONS

Tribology issues affect the reliable operation of MEMS devices and need to be understood on the micro/nanoscale. Tribological properties of materials and lubricants for MEMS devices need to be evaluated to identify the best candidates for MEMS. A summary of various tribological studies pertaining to MEMS has been thus far presented. It was seen that AFM/FFM-based techniques can be satisfactorily used to study and evaluate micro/nanoscale tribological phenomena related to MEMS devices. Such studies are necessary to herald the widespread impact of MEMS in the industry and our everyday lives.

## 6 REFERENCES

- [1] Trimmer, W. S. ed.: Micromachines and MEMS, Classic and Seminal Papers to 1990: IEEE Press 1993.
- [2] Kovacs, G. T. A.: Micromachined Transducers Sourcebook: WCB McGraw-Hill 1998.
- [3] Madou, M.: Fundamentals of Microfabrication: CRC Press 1997.
- [4] Bhushan, B. ed.: Tribology Issues and Opportunities in MEMS: Kluwer Academic 1998.
- [5] Bhushan, B.: Tribology and Mechanics of Magnetic Storage Devices, Second ed.: Springer-Verlag 1996.
- [6] Tai, Y. C., Fan, L. S., and Muller, R. S.: IC-Processed Micro-Motors: Design, Technology and Testing: Proc. IEEE Micro Electro Mechanical Systems 1989, 1-6.
- [7] Mehregany, M., Gabriel, K. J., and Trimmer, W. S. N.: Integrated Fabrication of Polysilicon Mechanisms: IEEE Trans. Electron Devices. (1988) 35, 719-723.
- [8] Hornbeck, L. J.: A Digital Light Processing(tm) Update - Status and Future Applications (Invited): Proc. Soc. Photo-Opt. Eng. (1999) 3634, Projection Displays V, 158-170.
- [9] Henck, S. A.: Lubrication of Digital Micromirror Devices: Tribol. Lett. (1997) 3, 239-247.
- [10] Horsley, D. A., Cohn, M. B., Singh, A., Horowitz, R., and Pisano, A. P.: Design and Fabrication of an Angular Microactuator for Magnetic Disk Drives: J. Microelectromech. Syst. (1998) 7, 141 - 148.
- [11] Miu, D. K. and Tai, Y. C.: Silicon Micromachined Scaled Technology: IEEE Trans. Industr. Electron. (1995) 42, 234-239.
- [12] Fan, L. S., Ottesen, H. H., Reiley, T. C., and Wood, R. W.: Magnetic Recording Head Positioning at Very High Track Densities Using a Microactuator-based, Two-stage Servo System: IEEE Trans. Ind. Electron. (1995) 42, 222-233.

- [13] Core, T. A., Tsang, W. K., and Sherman, S. J.: Fabrication Technology for an Integrated Surface-Micromachined Sensor: *Solid State Technol.* (1993 Oct) 36, 39-47.
- [14] Sulouff, R. E.: MEMS Opportunities in Accelerometers and Gyros and the Microtribology Problems Limiting Commercialization: Tribology Issues and Opportunities in MEMS. ed. B. Bhushan: Kluwer 1998, 109-120.
- [15] Guckel, H. and Burns, D. W.: Fabrication of Micromechanical Devices from Polysilicon Films with Smooth Surfaces: *Sensors and Actuators* (1989) 20, 117-122.
- [16] Mastrangelo, C. H. and Hsu, C. H.: Mechanical Stability and Adhesion of Microstructures Under Capillary Forces: *J. Microelectromech. Syst.* (1993) 2, 33-55.
- [17] Maboudian, R. and Howe, R. T.: Critical Review: Adhesion in Surface Micromechanical Structures: *J. Vac. Sci. Technol. B* (1997) 15, 1-20.
- [18] Bhushan, B., Israelachvili, J. N., and Landman, U.: Nanotribology: Friction, Wear and Lubrication at the Atomic Scale: *Nature* (1995) 374, 607-616.
- [19] Bhushan, B. ed.: *Handbook of Micro/Nanotribology*, Second ed.: CRC Press 1999.
- [20] Tong, L., Mehregany, M., and Matus, L. G.: Mechanical Properties of 3C Silicon Carbide: *Appl. Phys. Lett.* (1992) 60, 2992-2994.
- [21] Mehregany, M., Zorman, C. A., Rajan, N., and Wu, C. H.: Silicon Carbide MEMS for Harsh Environments: *Proc. IEEE* (1998) 86, 1595-1610.
- [22] Zorman, C. A., Fleischmann, A. J., Dewa, A. S., Mehregany, M., Jacob, C., Nishino, S., and Pirouz, P.: Epitaxial Growth of 3C-SiC Films on 4 in. Diam Si(100) Silicon Wafers by Atmospheric Pressure Chemical Vapor Deposition: *J. Appl. Phys.* (1995) 78, 5136-5138.
- [23] Zorman, C. A., Roy, S., Wu, C. H., Fleischman, A. J., and Mehregany, M.: Characterization of Polycrystalline Silicon Carbide Films Grown by Atmospheric Pressure Chemical Vapor Deposition on Polycrystalline Silicon: *J. Mater. Res.* (1998) 13, 406-412.
- [24] Gupta, B. K., Chevallier, J., and Bhushan, B.: Tribology of Ion Bombarded Silicon for Micromechanical Applications: *ASME J. Tribol.* (1993) 115, 392-399.
- [25] Gupta, B. K., Bhushan, B., and Chevallier, J.: Modification of Tribological Properties of Silicon by Boron Ion Implantation: *Tribol. Trans.* (1994) 37, 601-607.
- [26] Gupta, B. K. and Bhushan, B.: Nanoindentation Studies of Ion Implanted Silicon: *Surface and Coatings Technol.* (1994) 68-69, 564-570.
- [27] Bhushan B. and Koinkar, V.N.: Tribological Studies of Silicon for Magnetic Recording Applications: *J. Appl. Phys.* (1994) 75, 5741-5746.
- [28] Pharr, G. M.: The Anomalous Behavior of Silicon During Nanoindentation: In *Thin Films: Stresses and Mechanical Properties III*. eds. W.D. Nix, J.C. Bravman, E. Arzt and L.B. Freund: Materials Research Soc. 1991, 301-312.
- [29] Callahan, D. L. and Morris, J. C.: The Extent of Phase Transformation in Silicon Hardness Indentation: *J. Mater. Res.* (1992) 7, 1612-1617.
- [30] Sargent, P. M.: Use of the Indentation Size Effect on Microhardness for Materials Characterization: In *Microindentation Techniques in Materials Science and Engineering STP 889*. eds. P.J. Blau and B.R. Lawn: ASTM 1986, 160-174.
- [31] Bhushan, B. and Venkatesan, S.: Friction and Wear Studies of Silicon in Sliding Contact with Thin-Film Magnetic Rigid Disks. *J. Mater. Res.* (1993) 8, 1611-1628
- [32] Venkatesan, S. and Bhushan, B.: The Role of Environment in the Friction and Wear of Single-crystal Silicon in Sliding Contact with Thin-Film Magnetic Rigid Disks: *Adv. Info Storage Syst.* (1993) 5, 241-257.
- [33] Venkatesan, S. and Bhushan, B.: The Sliding Friction and Wear Behavior of Single-Crystal, Polycrystalline and Oxidized Silicon: *Wear* (1994) 171, 25-32.
- [34] Bhushan, B.: Chemical, Mechanical and Tribological Characterization of Ultra-Thin and Hard Amorphous Carbon Coatings as Thin as 3.5 nm: *Recent Developments: Diamond and Related Materials* (1999) 8, 1985-2015.
- [35] Bhushan, B., Sundararajan, S., Li, X., Zorman, C. A., and Mehregany, M.: "Micro/Nanotribological Studies of Single-Crystal Silicon and Polysilicon and SiC Films for Use in MEMS Devices", *Tribology Issues and Opportunities in MEMS* ed. Bhushan: Kluwer Academic 1998, 407-430.
- [36] Sundararajan, S. and Bhushan, B.: Micro/Nano tribological Studies of Polysilicon and SiC Films for MEMS Applications: *Wear* (1998) 217, 251-261.
- [37] Li, X. and Bhushan, B.: Micro/Nanomechanical Characterization of Ceramic Films for Microdevices: *Thin Solid Films* (1999) 340, 210-217.
- [38] Bhushan, B.: *Principles and Applications of Tribology*: Wiley 1999.
- [39] Yasseen, A. A., Wu, C. H., Zorman, C. A., and Mehregany, M.: Fabrication and Testing of Surface Micromachined Polycrystalline SiC Micromotors: *IEEE Elect. Dev. Lett.* (2000) 21, 164-166.
- [40] Bhushan, B., Kulkarni, A. V., Koinkar, V. N., Boehm, M., Odoni, L., Martelet, C., and Belin, M.: Microtribological Characterization of Self-Assembled and Langmuir-Blodgett Monolayers by Atomic Force and Friction Force Microscopy: *Langmuir* (1995) 11, 3189-3198.
- [41] Koinkar, V. N. and Bhushan, B.: Micro/nanoscale Studies of Boundary Layers of Liquid Lubricants for Magnetic Disks: *J. Appl. Phys.* (1996) 79, 8071-8075.
- [42] Koinkar, V. N. and Bhushan, B.: Microtribological Studies of Unlubricated and Lubricated Surfaces Using Atomic Force/Friction Force Microscopy: *J. Vac. Sci. Technol. A* (1996) 14, 2378-2391.

- [43] Bhushan, B. and Liu, H.: Nanotribological Properties and Mechanisms of Alkylthiol and Biphenyl Thiol Self-assembled Monolayers Studied by AFM: *Phys. Rev.* (2001) in press.
- [44] Bhushan, B.: Self-Assembled Monolayers for Controlling Hydrophobicity and/or Friction and Wear. In: *Modern Tribology Handbook* ed. B. Bhushan: CRC 2001, 909-930.
- [45] Sundararajan, S. and B. Bhushan: Topography-Induced Contributions to Friction Forces Measured Using an Atomic Force/Friction Force Microscope: *J. Appl. Phys.* (2000) 88, 4825-4831.
- [46] Tai, Y. C. and Muller, R. S.: Frictional Study of IC Processed Micromotors: *Sensors and Actuators A* (1990) 21-23, 180-183.
- [47] Gabriel, K. J., Behi, F., Mahadevan, R., and Mehregany, M.: In Situ Friction and Wear Measurement in Integrated Polysilicon Mechanisms: *Sensors and Actuators A* (1990) 21-23, 184-188.
- [48] Lim, M. G., Chang, J. C., Schultz, D. P., Howe, R. T., and White, R. M.: Polysilicon Microstructures to Characterize Static Friction: *Proc. IEEE Micro Electro Mechanical Systems* 1990, 82-88.
- [49] Beerschwinger, U., Yang, S. J., Reuben, R. L., Taghizadeh, M. R., and Wallrabe, U.: Friction Measurements on LIGA-Processed Microstructures: *J. Micromech. Microeng.* (1994) 4, 14-24.
- [50] Matheison, D., Beerschwinger, U., Young, S. J., Rueben, R. L., Taghizadeh, M., Eckert, S., and Wallrabe, U.: Effect of progressive wear on the friction characteristics of nickel LIGA processed rotors: *Wear* (1996) 192, 199-207.
- [51] Sundararajan, S. and Bhushan, B.: Static friction and surface roughness studies of surface micromachined electrostatic micromotors using an atomic force/friction force microscope: *J. Vac. Sci. Technol.* (2000) in press.